Fast 3D reconstruction of dental cast model based on structured light*

SONG Li-mei (宋丽梅)[1], **LIN Wen-wei** (林文伟)[1], **YANG Yan-gang** (杨燕罡)[2], **ZHU Xin-jun** (朱新军)[1], **GUO Qing-hua** (郭庆华)[1,3]**, **and YANG Huai-dong** (杨怀栋)[4]

1. Key Laboratory of Advanced Electrical Engineering and Energy Technology, Tianjin Polytechnic University, Tianjin 300387, China

2. School of Mechanical Engineering, Tianjin University of Technology and Education, Tianjin 300222, China

3. School of Electrical, Computer and Telecommunications Engineering, University of Wollongong, Wollongong 2500, Australia

4. Department of Precision Instrument, Tsinghua University, Beijing 100084,China

(Received 18 May 2018; Revised 2 July 2018)

To quickly obtain accurate 3D data of dental cast model, this paper proposes a 3D reconstruction method for dental cast model based on structured light. This method combines the structured light with the motor turntable to obtain a group of 3D data for the dental cast model from multiple angles, and automatically registers the dental 3D data from multiple angles through the ball calibration of turntable. Compared with the real data of the dental cast model, the maximum error of the 3D reconstruction results in this paper is 0.115 mm. The reconstruction time of this process is about 130 s. The experimental results show that the method has high precision and high scanning speed for the 3D reconstruction of the dental cast model.

Document code: A **Article ID:** 1673-1905(2018)06-0457-4

DOI https://doi.org/10.1007/s11801-018-8076-z

The traditional dental cast model production has problems such as complicated production process, low production efficiency, and difficulty in preservation. Compared with the traditional method, the non-contact optical 3D measurement method greatly shortens the measurement time, provides more accurate data aided design for the dental cast model, and is beneficial to data management and recording[1]. The commonly used optical 3D measurement methods include time flight method, structured light projection method, laser 3D scanning method and binocular vision method. The time flight method uses time flight cameras to acquire 3D data of objects. It is not affected by the grayscale and object characteristics of objects, and the accuracy of depth calculation does not vary with the distance. However, the time flight camera has low resolution and high cost. The laser 3D scanning method has high accuracy and high point cloud data density, but it is with high cost and slow measurement speed[2]. The 3D non-contact measurement technology based on structured light has high measurement speed, low cost, and good stability[3]. Ou et al proposed a 3D dental measurement system based on structured light. This method can only achieve 3D reconstruction of an angle[4]. Chen et al proposed a new digital dental laser scanning system, but the cost is too high and the accuracy is insufficient[5]. On the basis of the previous research in our laboratory[6,7], this paper proposes a fast 3D reconstruction method for dental cast model based on structured light. Compared with the above methods, this method solves the problem of rapid and accurate reconstruction of a 3D dental cast model.

This paper uses the three wavelength phase shift profilometry (TWPSP) method[8] to reconstruct 3D data of the dental cast model, which has been done in the previous research. In the TWPSP method, the wrapped phase can be obtained with three proper wavelengths directly. Therefore, the noise enhancement problem is alleviated. Moreover, it does not need to calculate the equivalent phase maps, so the speed is higher.

The TWPSP method uses a grating stripe with wavelengths λ_1=1 008 pixel, λ_2=144 pixel, and λ_3=16 pixel to project the object to be measured. The phase shift between adjacent fringe patterns is $\frac{\pi}{3}$, which takes six

* This work has been supported by the National Natural Science Foundation of China (Nos.61078041 and 51806150), the Natural Science Foundation of Tianjin (Nos.16JCYBJC15400, 15JCYBJC51700 and 18JCQNJC04400), the State Key Laboratory of Precision Measuring Technology and Instruments (Tianjin University) (PIL1603), the Program for Innovative Research Team in University of Tianjin (No.TD13-5036), and Tianjin Enterprise Science and Technology Commissioner Project (No.18JCTPJC61700).

** E-mail: qguo@uow.edu.au

raster images with phase shifts of 0, $\frac{\pi}{3}$, $\frac{2\pi}{3}$, π, $\frac{4\pi}{3}$ and $\frac{5\pi}{3}$. The gray values of the collected images are $I_1(x,y)$, $I_2(x,y)$, $I_3(x,y)$, $I_4(x,y)$, $I_5(x,y)$, $I_6(x,y)$. The phase value $\phi_i(x,y)$ at this time can be obtained by

$$\phi_i(x,y)=\tan^{-1}\left(\frac{I_3(x,y)-I_5(x,y)}{I_4(x,y)-I_1(x,y)+I_3(x,y)-I_5(x,y)}\right) \quad i=1,2,3. \tag{1}$$

The unwrapped phase value $\Phi_3(x,y)$ can be solved according to

$$\Phi_3(x,y)=\phi_3(x,y)+2\pi\times \left\{\mathrm{INT}\left(\frac{\phi_3(x,y)}{2\pi}\times N_1\right)\times N_2+\mathrm{INT}\left(\frac{\phi_2(x,y)}{2\pi}\times N_2\right)\right\}, \tag{2}$$

where INT( ) is rounding function.

When $\phi_3(x,y)$ is 2π, phase transitions may occur, so the error correction for the phase unwrapping operation described in Eq.(2) is used as follows.

When $\phi_1(x,y)\neq 2\pi$ and $\phi_2(x,y)\neq 2\pi$, and $\phi_3(x,y)\neq 2\pi$, the unwrapped phase value $\Phi_3(x,y)$ is corrected by

$$\Phi_3(x,y)=\phi_3(x,y)+2\pi\times \left\{\mathrm{INT}\left(\frac{\phi_1(x,y)}{2\pi}\times N_1\right)\times N_2+\mathrm{INT}\left(\frac{\phi_2(x,y)}{2\pi}\times N_2\right)\right\}. \tag{3}$$

When $\phi_1(x,y)\neq 2\pi$, and $\phi_2(x,y)=2\pi$ or $\phi_3(x,y)=2\pi$, the unwrapped phase value $\Phi_3(x,y)$ is corrected by

$$\Phi_3(x,y)=\phi_3(x,y)+2\pi\times \left\{\mathrm{INT}\left(\frac{\phi_1(x,y)}{2\pi}\times N_1\right)\times N_2+\mathrm{INT}\left(\frac{\phi_2(x,y)}{2\pi}\times N_2\right)-1\right\}. \tag{4}$$

When $\phi_1(x,y)=2\pi$, $\phi_2(x,y)\neq 2\pi$ and $\phi_3(x,y)\neq 2\pi$, the unwrapped phase value $\Phi_3(x,y)$ is corrected by

$$\Phi_3(x,y)=\phi_3(x,y)+2\pi\times \left\{\mathrm{INT}\left(\frac{\phi_1(x,y)}{2\pi}\times N_1-1\right)\times N_2+\mathrm{INT}\left(\frac{\phi_2(x,y)}{2\pi}\times N_2\right)\right\}, \tag{5}$$

where $N_1=\lambda_1/\lambda_2$, $N_2=\lambda_2/\lambda_3$.

In order to realize automatic merging of 3D data of dental cast model, we need to know the rigid transformation of each image with respect to a common coordinate system. Prior to this, we have completed camera calibration of the binocular 3D reconstruction system[9]. As shown in Fig.1, we define three independent coordinate systems in 3D space, the world coordinate system (WCS), the camera coordinate system (CCS) and the turntable coordinate system (TCS), whose origins are O_w, O_c and O_s, respectively. We have previously known that the transformation $\boldsymbol{T}_{cw}$, which is from the origin of the WCS O_w to that of the CCS O_c, is before the camera calibration. If we know the transformation $\boldsymbol{T}_{ws}$ that is from the origin of the TCS O_s to that of the WCS O_w, we can derive the transformation

$$\boldsymbol{T}_{cs}=\boldsymbol{T}_{cw}\boldsymbol{T}_{ws}=\begin{bmatrix}\boldsymbol{R}_{cw} & \boldsymbol{t}_{cw}\\ \boldsymbol{0}^T & \boldsymbol{1}\end{bmatrix}\begin{bmatrix}\boldsymbol{R}_{ws} & \boldsymbol{t}_{ws}\\ \boldsymbol{0}^T & \boldsymbol{1}\end{bmatrix}, \tag{6}$$

where $\boldsymbol{R}_{cw}$ and $\boldsymbol{R}_{ws}$ are orthogonal rotation matrices. The values of $\boldsymbol{R}_{cw}$ and $\boldsymbol{t}_{cw}$ have been obtained by camera calibration.

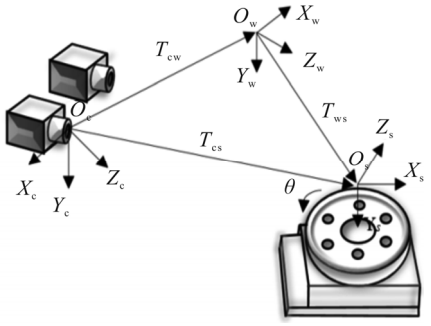

Fig.1 Geometry of the vision system

As shown in Fig.2, suppose there is a 3D point p_0 in WCS (set it on O_w, but it is not necessary) and p_0' is the same point after being rotated by angle θ along the $\boldsymbol{Y}_s$ axis of the turntable. Given two 3D points and the rotation axis $\boldsymbol{Y}_s$, we can define a plane Π as shown in the figure. Then we know the vector product

$$(p_0'-p_0)\cdot\boldsymbol{Y}_s=0. \tag{7}$$

In other words,

$$\begin{bmatrix}p_{0x}'-p_{0x}\\ p_{0y}'-p_{0y}\\ p_{0z}'-p_{0z}\end{bmatrix}^T\begin{bmatrix}\boldsymbol{Y}_{sx}\\ \boldsymbol{Y}_{sy}\\ \boldsymbol{Y}_{sz}\end{bmatrix}=0 \quad . \tag{8}$$

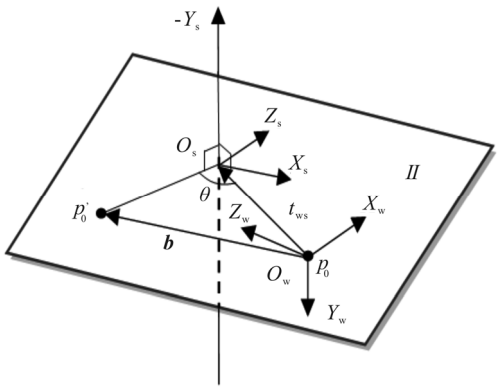

Fig.2 Rotation axis calibration with respect to the WCS

When we have at least three points in the world coordinates, we can use the SVD technique to solve the over determined linear equations[10]

$$\boldsymbol{AY}=\begin{bmatrix}p_{0x}'-p_{0x} & p_{0y}'-p_{0y} & p_{0z}'-p_{0z}\\ p_{1x}'-p_{1x} & p_{1y}'-p_{1y} & p_{1z}'-p_{1z}\\ & \cdots & \\ p_{Nx}'-p_{Nx} & p_{Ny}'-p_{Ny} & p_{Nz}'-p_{Nz}\end{bmatrix}\begin{bmatrix}\boldsymbol{Y}_{sx}\\ \boldsymbol{Y}_{sy}\\ \boldsymbol{Y}_{sz}\end{bmatrix}=0. \tag{9}$$

When matrix $\boldsymbol{A}$ is decomposed as $\boldsymbol{A}=(\boldsymbol{UDV}^T)$, the solution of the equation is a column vector of $\boldsymbol{V}$ that corresponds to the column of the least eigenvalue in the $\boldsymbol{D}$ matrix. We normalize the vector $\boldsymbol{Y}_s$ to $\hat{\boldsymbol{Y}}_s$. We initialize the $\boldsymbol{X}$ axis to (1.0, X_{sy},1.0), then calculate the $\boldsymbol{X}_s$ axis and the $\boldsymbol{Z}_s$ axis of TCS.

$$\begin{aligned} \boldsymbol{X}_{\mathrm{s}} \times \boldsymbol{Y}_{\mathrm{s}} &= \boldsymbol{0}, \\ \boldsymbol{X}_{\mathrm{sy}} &= (-\boldsymbol{X}_{\mathrm{sx}} \boldsymbol{Y}_{\mathrm{sx}} - \boldsymbol{X}_{\mathrm{sx}} \boldsymbol{Y}_{\mathrm{sz}}) / \boldsymbol{Y}_{\mathrm{sy}}, \\ \hat{\boldsymbol{X}}_{\mathrm{s}} &= \boldsymbol{X}_{\mathrm{s}} / \left\| \boldsymbol{X}_{\mathrm{s}} \right\|, \\ \hat{\boldsymbol{Z}}_{\mathrm{s}} &= \hat{\boldsymbol{X}}_{\mathrm{s}} \times \hat{\boldsymbol{Y}}_{\mathrm{s}}. \end{aligned} \tag{10}$$

Finally, the rotation matrix from the turntable to the WCS is defined as

$$\boldsymbol{R}_{\mathrm{ws}} = \begin{bmatrix} (\hat{\boldsymbol{X}}_{\mathrm{s}})^{\mathrm{T}} \\ (\hat{\boldsymbol{Y}}_{\mathrm{s}})^{\mathrm{T}} \\ (\hat{\boldsymbol{Z}}_{\mathrm{s}})^{\mathrm{T}} \end{bmatrix}^{\mathrm{T}}. \tag{11}$$

Suppose the two points p_0 and p_0' are transformed, with respect to the TCS, to new points $p_{\mathrm{s}0}$ and $p_{\mathrm{s}0}$', respectively. Then the three points O_{s}, $p_{\mathrm{s}0}$ and $p_{\mathrm{s}0}$' are on the Π plane and form an isosceles triangle. Therefore, using a vector $\boldsymbol{b}$=$p_{\mathrm{s}0}$'− $p_{\mathrm{s}0}$, where ($p_{\mathrm{s}0}$, $p_{\mathrm{s}0}$')=$\boldsymbol{R}_{\mathrm{ws}}{}^{\mathrm{T}}$($p_0$, p_0'), and the rotation angle θ, we can compute a transformation vector $\boldsymbol{t}_{\mathrm{ws}}$ from $p_{\mathrm{s}0}$ to the origin O_{s}.

Let us consider the Π plane on which the origin is moved to $p_{\mathrm{s}0}$. Then the center of rotation intersects with Π at a 3D point $\boldsymbol{t}_i$=[x,0.0,z]$^{\mathrm{T}}$. Because the isosceles triangle is also on the plane, the origin $\boldsymbol{t}_i$ is one of the intersection points of the two circles c_1 and c_2 as shown in Fig.3. On the Π plane, the center of c_1 is at [0.0,0.0,0.0]$^{\mathrm{T}}$ and its diameter is $\| \boldsymbol{t}_i \|$. Similarly, the center of c_2 is at [b_x,0.0,b_z]$^{\mathrm{T}}$ and its diameter is also $\| \boldsymbol{t}_i \|$. Let r= $\| \boldsymbol{t}_i \|$ and b=$\|\boldsymbol{b}\|$, then we derive two circles' equations as

$$\begin{aligned} & x^2 + z^2 = r^2, \\ & (x - b_x)^2 + (z - b_z)^2 = r^2. \end{aligned} \tag{12}$$

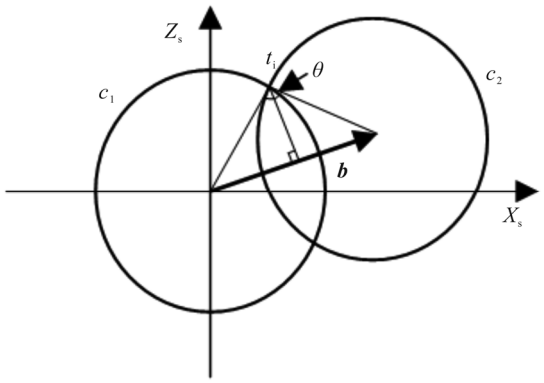

Fig.3 Intersection of two rotations

Let us now derive the transformation matrix from the TCS to the CCS. Because we shift the origin O_{s} to point $p_{\mathrm{s}0}$ to find point $\boldsymbol{t}_i$, the translation from O_{w} to O_{s} becomes $-(\boldsymbol{t}_i+p_{\mathrm{s}0})$ with respect to the TCS and $-\boldsymbol{R}_{\mathrm{ws}}(\boldsymbol{t}_i+p_{\mathrm{s}0})$ with respect to the WCS. Finally, the transformation from the turntable to the CCS is computed as

$$\boldsymbol{T}_{\mathrm{cs}} = \begin{bmatrix} \boldsymbol{R}_{\mathrm{ws}} & -\boldsymbol{R}_{\mathrm{ws}}(\boldsymbol{t}_i + p_{\mathrm{s}0}) \\ \boldsymbol{0}^{\mathrm{T}} & \boldsymbol{1} \end{bmatrix}. \tag{13}$$

After the calibration of the turntable is completed, a standard ball with a diameter of 20(± 0.001) mm is used as a calibration tool. The center of standard ball is fitted with the least square method[11]. Six groups of 3D data are acquired by rotating the turntable to complete the ball turntable correction. Fig.4 shows the results of standard ball multi-angle 3D data and standard ball fitting.

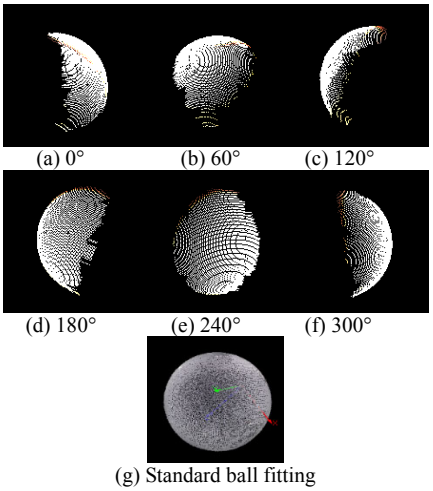

Fig.4 3D multi-angle images of the standard ball

We use the Geomagic studio to measure the diameter of the 3D data of the standard ball. The measured diameter error is shown in Tab.1. We creat a 3D sphere model with a diameter of 20(± 0.000 1) mm and spherically fit it to the standard ball 3D data by Geomagic studio, as shown in Fig.5.

Tab.1 Ball radius error comparison

Ball border (mm)	Ball diameter (mm)	Error (mm)
X:[31.806 108,51.949 169]	20.143 061	0.143 061
Y:[38.865 998,58.894 619]	20.028 621	0.028 621
Z:[-54.896 941,-34.778 673]	20.118 268	0.118 268

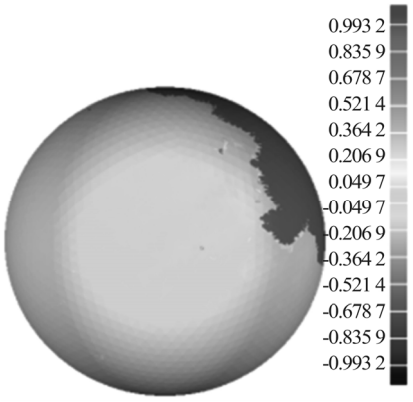

Fig.5 Spherical fitting by Geomagic studio

The average error of the standard ball diameters obtained through the *X*-axis, *Y*-axis, and *Z*-axis is 0.096 65 mm. Since some of the data in the *Y*-axis direction cannot be measured under the motor turntable, the value in the direction is greatly deviated. The standard deviation of the spherical fitting is 0.034 0 mm and the

root mean square (*RMS*) is 0.045 6 mm.

After the ball calibration of the turntable, the TWPSP method is used to analyze the fringe pattern and reconstruct the 3D data. This has been done in previous studies.

The binocular 3D reconstruction system is shown in Fig.6, where an LG (HX300G) resolution of 1 024×768 is used to cast three frequency cosine white stripes. The industrial camera (rs-A13 000gm/gc) sends a 1 280×1 024 gray image to the computer at a frame rate of 4 frames/s. The industrial camera uses an 8 mm (M0814-MP2) lens. The motor turntable (ERSP100) is controlled by a motor controller (PMC100). The system is about 500 mm away from the measured object when measuring the dental cast model, and the angle between the two cameras is 60°. The measuring range of this system is about 450 mm.

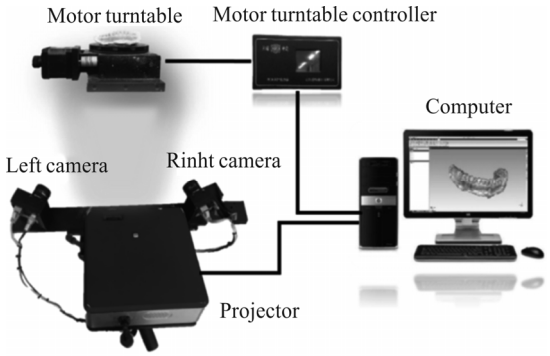

Fig.6 The binocular 3D reconstruction system

The 3D data of the six perspectives of the dental cast model and reconstruction result are shown in Fig.7

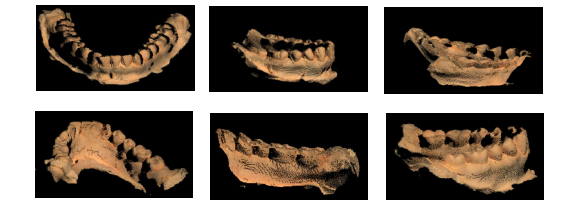

(a) 3D point cloud data of six different angles

(b) 3D data of different angles

(c) Original pictures of the dental cast model

Fig.7 Registration results of six images

We use LJ-V7000 (measurement accuracy is up to 5 μm) to collect the 3D data of the dental cast model and use it as the real value. We measure the distance between any two features of the dental model by Geomagic studio and compare it to the actual value. The results are shown in Tab.2. The average error of the five groups of data is 0.067 4 mm and the maximum error is 0.115 mm, which satisfies the allowable error range of the dental cast model. In view of the computation time, the proposed method takes about 130 s to complete the whole process and the total process is without manual involvement.

Tab.2 3D measurement data and actual values

X axis (mm)	*Y* axis (mm)	*Z* axis (mm)	3D data (mm)	Actual value (mm)	Error (mm)
16.388	0.722	0.948	16.431	16.54	0.109
28.779	1.032	5.801	29.376	29.44	0.064
36.276	1.230	14.519	39.093	39.12	0.027
8.219	5.210	9.806	13.815	13.70	-0.115
4.738	2.417	3.452	6.342	6.32	-0.022

A fast 3D reconstruction of dental cast model based on structured light method is proposed in this paper. Firstly, the ball calibration of the turntable is performed on the basis of the calibration of the binocular stereo camera. Secondly, the rotating object of the motor turntable is obtained from multi-angle 3D point cloud data. Finally, the multi-angle point cloud data are then registered and integrated into a 3D model. The experimental results show that the method can implement the multi-angle 3D reconstruction of the dental cast model in a short time, and the reconstruction accuracy of the method can meet the precision requirements of the dental cast model 3D reconstruction.

References

[1] Adaškevičius R and Vasiliauskas A, Electronics and Electrical Engineering **82**, 49 (2015).

[2] Gao Yan, Shao Shuangyun and Feng Qibo, Chinese Journal of Lasers **40**, 182 (2013).

[3] J. Geng, Advances in Optics and Photonics **3**, 128 (2011).

[4] Ou Pan, Wang Ting and Li Ruixiang, Laser & Optoelectronics Progress **53**, 121 (2016). (in Chinese)

[5] Chen Xinqi, Hu Ying, Ma Wei and Nie Jianhui, Journal of Harbin Institute of Technology **44**, 11 (2012). (in Chinese)

[6] L. M. Song, P. Q. Wang, Y. L. Chang, X. J. Li, J. T. Xi, Q.H. Guo and B.N. Li, Optoelectronics Letters **11**, 145 (2015).

[7] L.M. Song, D.P. Li, M.C. Qin, Z.Y. Li, Y.L. Chang and J.T. Xi, Optoelectronics Letters **10**, 378 (2014).

[8] Limei Song, Yulan Chang, Jiangtao Xi, Qinghua Guo, Xinjun Zhu and Xiaojie Li, Optics Communications **35**, 213 (2015).

[9] Z. Zhang, IEEE Transaction Pattern Analysis and Machine Intelligence **22**, 1330 (2000).

[10] Soon-Yong Park and Murali Subbarao, Machine Vision and Applications **16**, 148 (2005).

[11] S. Theodoridis, The Least-Squares Family, 6th ed., Academic Press, Oxford (2015).